JTTEE5 17:478–485
DOI: 10.1007/s11666-008-9200-6
1059-9630/$19.00 © ASM International

Microstructure and Thermal Behavior of Thermal Barrier Coatings

E. Garcia, P. Miranzo, R. Soltani, and T. W. Coyle

(Submitted January 11, 2008; in revised form April 18, 2008)

Yttria stabilized zirconia thick coatings were thermally sprayed from two different feedstock powders. Coating characteristics such as density, crystalline phase composition, and microstructure were evaluated. The thermal expansion coefficient and thermal diffusivity were measured as a function of temperature up to 800 °C and analyzed in terms of the microstructural features. The ability of available models to relate the measured thermal properties to the microstructural features as characterized by readily available methods was assessed. The importance of pore shape and orientation on the thermal conductivity was evidenced. The thermal contact resistance between the substrate and the coating in these samples was estimated from the thermal diffusivity data, and found to change during cooling from 800 °C.

Keywords microstructure, plasma spray, thermal conductivity, thermal barrier coatings, zirconia

1. Introduction

Thermally sprayed yttria partially stabilized zirconia (Y-PSZ) has been widely used as a thermal barrier coating (TBC) to protect metallic parts exposed to the hot gas stream in gas turbine engines used for aircraft propulsion and power generation. The use of TBCs 100 to 500 μm thick reduces the surface temperature of the metallic components, providing good performance at temperatures as high as 1000 °C (Ref 1-3). In the case of Diesel engines, thermal barrier coatings have been pursued to increase the working temperature in the combustion chamber from 400 to ~900 °C (Ref 4, 5). In this way, the thermal efficiency of the Diesel process is improved, reducing the fuel consumption and emissions of hazardous combustion products. In this application, significantly thicker coatings (~1 mm) are required than for turbine blades.

The thermal conductivity of the TBCs greatly depends on the material microstructure, which is characterized by the existence of splats and pores of different shapes and sizes. The size, shape, orientation, and relative amounts of these features are directly related to the coating deposition technique, the process parameters, and the morphology of the powder feedstock (Ref 6-8). The reduction in thermal conductivity due to the presence of pores was described by Maxwell for spherical noninteracting pores, with the following expression (Ref 9):

$$f_1[P] = \frac{k_{\text{Porous}}}{k_{\text{Dense}}} = 1 - \frac{3}{2}P \qquad \text{(Eq 1)}$$

where P is the volume fraction of spherical porosity. In most cases, the reduction in conductivity cannot be adequately explained by this expression; the pore shape has to be considered as well. Several models have been developed considering the pore shape (Ref 10-12). In thermal sprayed coatings, three different types of pores are commonly found: thin horizontal pores parallel to the substrate surface, thin vertical pores or cracks perpendicular to the substrate surface, and rounded pores. The effect of the thin horizontal pores can be estimated by the expression of Kachanov et al. (Ref 13, 14):

$$f_2[P_h] = \frac{k_{\text{Porous}}}{k_{\text{Dense}}} = 1 - \left(\frac{2 \cdot P_h}{\pi}\right) \cdot \left(\frac{l}{t}\right) \qquad \text{(Eq 2)}$$

where P_h is the volume fraction of horizontal pores and "l/t" is their average aspect ratio. The effect of vertical pores is often neglected as the heat flux typically runs parallel to those pores. If only the contributions of rounded (P_r) and thin horizontal pores (P_h) are considered and the scattering of phonons and radiation by the pores is taken as negligible (Ref 15, 16), the effective thermal conductivity of the coatings may be described by the expression (Ref 17):

$$\frac{k_{\text{Coating}}}{k_{\text{Dense}}} = \frac{1}{2}\left\{f_2\left[\frac{P_h}{1-P_r}\right] \cdot f_1[P_r] + f_1\left[\frac{P_r}{1-P_h}\right] \cdot f_2[P_h]\right\} \qquad \text{(Eq 3)}$$

where f_1 and f_2 represent the functions expressed by Eq. 1 and 2, respectively. This approach has been successfully employed to account for different pore shapes in modeling the thermal conductivity of plasma sprayed materials (Ref 17, 18). Other models include more detailed analysis of the effects of pore shape on the thermal conductivity; however, they require determination of specific microstructural parameters only measurable by techniques not readily accessible to most laboratories (Ref 7, 8).

E. Garcia and **P. Miranzo**, Institute for Ceramics and Glass (C.S.I.C.), C/Kelsen 5, Campus de Cantoblanco, 28049 Madrid, Spain; and **R. Soltani** and **T.W. Coyle**, Centre for Advanced Coating Technologies, University of Toronto, Toronto, ON Canada M5S 3E4. Contact e-mail: garcia@icv.csic.es.

Typically TBCs are separated from their substrate before measurement of the thermal diffusivity by grinding away the substrate or dissolving the substrate in acidic or caustic solutions. It would be convenient to be able to characterize the coating while it was still attached to the substrate, avoiding the difficult and time-consuming separation process and any damage to the coating that may occur during separation. More importantly, the interface between the thermal barrier and the metallic substrate is important to both the thermal and the mechanical performance of the TBC system. The flow of heat through the layered samples would be affected by the nature of the interface and any defects located there.

If measurements of heat flow through such a layered system are interpreted by simply assuming that the thermal properties are uniform throughout, an *apparent thermal diffusivity* is obtained. The variation in the thermal diffusivity from layer to layer can be accounted for by using the following expression to describe the heat diffusion through a two-layer sample:

$$\frac{\partial^2 \theta_j(z,t)}{\partial z^2} = \frac{1}{\alpha_j}\frac{\partial \theta_j}{\partial t} \quad j = 1,2 \qquad \text{(Eq 4)}$$

where α_j is the thermal diffusivity and θ_j is the temperature of the jth layer, and z is the distance from the interface. Assuming there is no contact resistance at the interface between the two layers ($z = 0$), this equation can be solved using the appropriate initial and boundary conditions (Ref 19):

$$k_1 \frac{\partial \theta_1(0,t)}{\partial z} = k_2 \frac{\partial \theta_2(0,t)}{\partial z} \qquad \text{(Eq 5)}$$

where k_1 and k_2 are the thermal conductivities of layer 1 and layer 2, respectively. An analytical solution for a two-layer medium with a thermal contact resistance, R_C, at the interface can be obtained from Eq. 4 by including a thermal contact resistance at the interface in the boundary conditions. In this case the expression of the boundary condition is:

$$-k_1 \frac{\partial \theta_1(0,t)}{\partial z} = -k_2 \frac{\partial \theta_2(0,t)}{\partial z} = \frac{c}{R_C}[\theta_1(0,t) - \theta_2(0,t)] \qquad \text{(Eq 6)}$$

where c is a constant that depends on the known thermal and physical properties of each layer. In this model, the thermal current density across the interface is related to the temperature drop across the interface. Both analytical models are implemented in the software of the equipment, and iterative computer routines have been used for evaluating the quality of the substrate/coating interface.

The influence of microstructural features on the thermal properties of air plasma sprayed Y-PSZ coatings deposited on mild steel substrates using two distinctive types of commercially available powders was investigated in this study. The use of the bond coat, typically employed in TBC applications, has been avoided to simplify the problem by modeling the thermal behavior of bi-layer systems. Readily available techniques such as x-ray diffraction, thermal dilatometry, scanning electron microscopy, and image analysis were used to characterize the microstructures. The thermal diffusivities of two-layer coating/substrate samples, freestanding coatings, and the substrate were measured using the laser flash method. The measured thermal conductivity of the coatings was compared with predictions from Eq. 1 to 3 to assess the ability of these models to describe the dependence of conductivity on porosity for these complex microstructures. Given the thermal conductivity of the substrate, the thermal conductivity of the coating can be obtained without separating it from the substrate, provided that the interfacial resistance was negligible or constant for a specific coating-substrate combination. The interfacial resistance for the samples investigated in this study was estimated by comparing the measured *apparent thermal diffusivity* of the steel/coating samples to an *apparent thermal diffusivity* calculated from the measured thermal properties of the coating and substrate.

2. Experimental

2.1 Sample Preparation

Two commercially available 6-8 wt.% Y_2O_3-PSZ powders were used to deposit coatings by air plasma spraying with a SG-100 Miller plasma torch on carbon steel substrates. The nanostructured powder was Nanox S4007 from Inframat Corp. (Willington, CT). This powder consists of agglomerated particles 15-150 μm in diameter made up of grains on the order of 200 nm. The morphology of the Nanox powder is shown in Fig. 1, with noticeable porosity within the agglomerated particles (Fig. 1 right).

The microstructure of the second powder used in this work, a HOSP™ (hollow oven spherical powder) 204B-NS powder (Sulzer Metco, NY, USA), is shown in Fig. 2. It consists of hollow spherical particles in the range 45-75 μm with excellent flowability. This type of powder is easy to melt during the plasma spray process due to the small thickness and high density of the shell (Fig. 2, right).

The substrates employed were thick carbon steel plates (4 mm thickness) to reduce the risk of deformation during spraying. The surface of the substrates was grit blasted before coating with alumina grit to an average roughness of approximately 4 μm as measured using a surfometer from Precision Devices Inc. (MI, USA).

A DPV2000 system (Tecnar, QC, Canada) was employed to set the deposition parameters used in this work. This device is an optical sensing instrument, which provides online monitoring of individual particle characteristics in thermal spray plumes and is able to measure and monitor temperature, size, and velocity distributions providing mean values and standard deviation of in-flight particles. The spraying parameters shown in Table 1 were selected to obtain an average particle temperature high enough to melt the Nanox powder, as the nanostructured particles are harder to melt than the HOSP™ because the intra-agglomerate nanoporosity limits the heat trans-

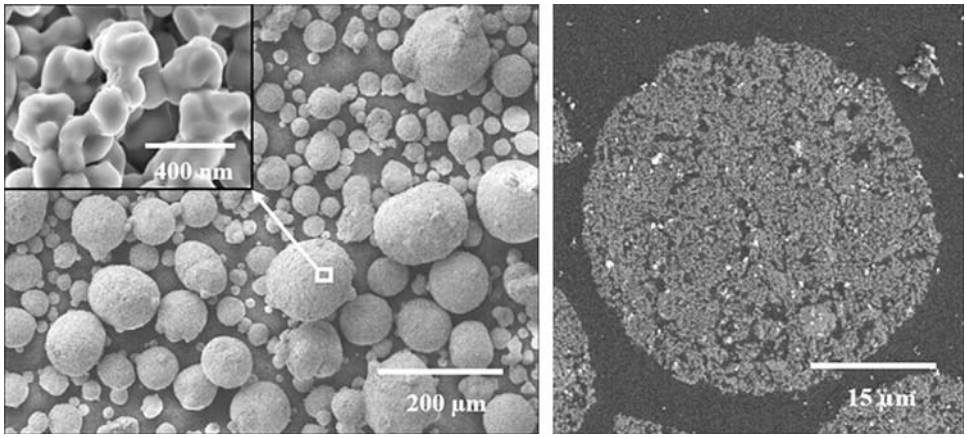

Fig. 1 SEM micrographs of Nanox feedstock showing the nanostructured morphology of the agglomerated particles (left) and a polished cross-sectional view of one particle (right)

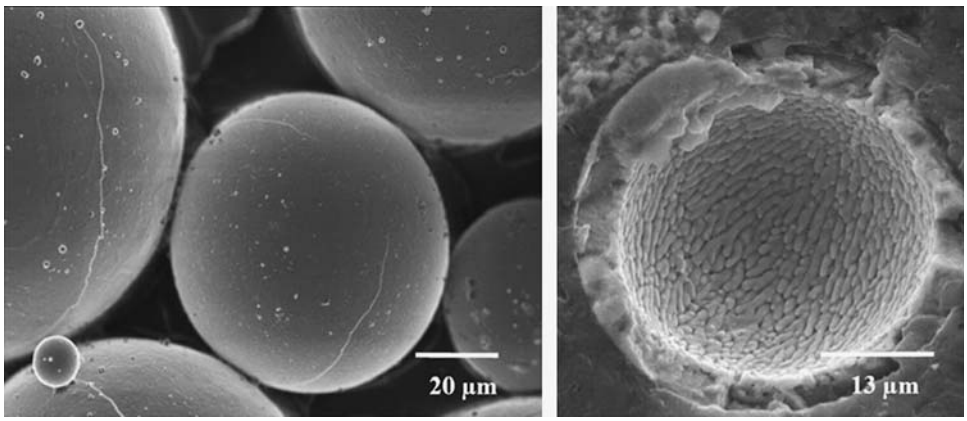

Fig. 2 SEM images of HOSP^{TM} 204B-NS feedstock particles (left) and a cross-sectional view of one of those particles showing a dense shell and hollow interior (right)

Table 1 Spraying parameters used for the Nanox feedstock

Parameters	
Power, kW	32.5
Current, A	740
Recorded voltage, V	44
Ar gas flow rate, l min^{-1}	40
H_2 gas flow rate, l min^{-1}	2
Ar carrier gas, l min^{-1}	8
Distance, cm	7
Mean velocity, m s^{-1}	226
Mean temperature, °C	2633

fer from the plasma to the powder. Due to this fact together with the bigger size of Nanox powders, it is expected to obtain coatings formed by less melted or spreaded splats. The values of the average temperature and velocity of the nanostructured powder obtained with the set of parameters given in Table 1 were 2633 °C and 226 m s^{-1}, respectively. The HOSP^{TM} 204B-NS powder was deposited with the same process parameters to compare the properties and microstructure of both coatings. Additional information about this type of coatings can be found in a previous paper published by the authors (Ref 20).

Freestanding coatings were obtained by immersing the specimens in a 40% HNO_3 solution for 1 h. The acid attacked the carbon steel/coating interface detaching the coating from the substrate.

2.2 Characterization

Phase analyses of powders and coatings were carried out by X-ray diffraction using a Philips model PW2273 diffractometer. The powders and coatings were examined by low voltage scanning electron microscopy (Hitachi S-4500). Quantitative image analysis was performed on SEM images (at least 10 micrographs per coating at 1000× magnification) using the image-analysis software LEICA QWIN (Leica Microsystem, Weztlar, Germany). The density of the freestanding coatings was measured by the Archimedes method using a high precision balance.

The linear thermal expansion coefficient was measured on bars of 3 mm in length machined from freestanding coatings in the direction perpendicular to the spraying axis using a vertical dilatometer (Setsys 16/18 Setaram Scientific & Industrial Equipment, Caluire, France).

The thermal diffusivity (α) was measured by the laser flash method (Ref 21) on 9 mm × 9 mm × 1 mm square samples. Layered samples (1 mm steel/1 mm coating), freestanding coatings, and the mild steel substrate were cut and machined from the original thick samples with a precision grinding wheel (Accutom-50, Struess, Germany) to accurately control the thickness. Data were taken from room temperature (RT) up to 800 °C, the maximum temperature expected in the diesel engine combustion chamber, (up to 600 °C for layered samples and the steel substrate), during both the heating and cooling cycle, using a Thermaflash 2200 system (Holometrix-Micromet, now Netzsch, Inc. Bedford, USA). Specimens were coated with a thin carbon layer before testing to prevent the direct transmission of the laser beam and to enhance absorption/emission at the specimen surface. The coefficient of variation of the thermal diffusivity measurement for a given coating by this laser flash technique was reported to be 6% (Ref 22). The thermal conductivity k was then calculated by the following expression:

$$k = \alpha \cdot \rho \cdot c \qquad \text{(Eq 7)}$$

where ρ is the measured density and c is the specific heat taken from the literature (Ref 23). The thermal conductivities of the coatings and substrate derived from the measured diffusivities were used to predict an *apparent thermal diffusivity* for the coating/substrate-layered system. This value was compared with the *apparent thermal diffusivity* measured for the layered sample. The difference between the predicted and measured apparent diffusivities was attributed to the interfacial resistance.

3. Results and Discussion

Both coatings showed good mechanical integrity with no signs of macrocracking or debonding from the substrates. Diffraction patterns of Nanox and HOSP™ powders and coatings are shown in Fig. 3. Nanox powder and coating were completely tetragonal. No peak broadening is observed in the pattern of the Nanox powder as the particles forming the powder agglomerates were not small enough to evidence that effect. The XRD pattern of the HOSP™ powder showed a small amount of monoclinic phase, which disappeared after spraying.

The thermal expansion coefficients of the Nanox and HOSP™ samples were constant in the measured temperature range (25-1000 °C), being 10.3×10^{-6} and 9.2×10^{-6} °C^{-1}, respectively. Both coatings were entirely tetragonal as sprayed and had essentially the same chemical composition; therefore, the difference in the thermal expansion behavior must be related to differences in porosity, which is a little bit higher in the case of the HOSP™ material.

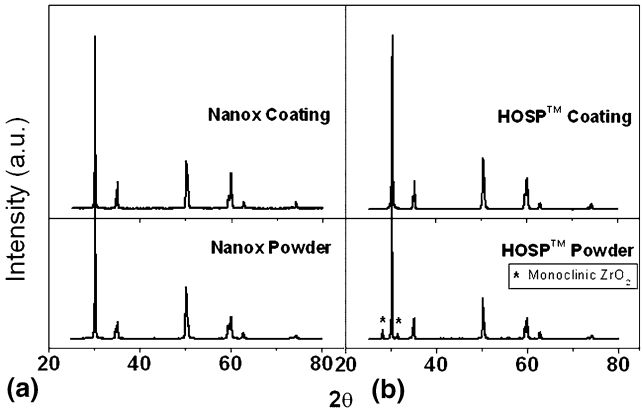

Fig. 3 X-ray diffraction patterns of Nanox (a) and HOSP™ (b) powders and coatings

The microstructure of the coatings was analyzed at different levels. In Fig. 4, polished cross sections of Nanox (Fig. 4a) and HOSP™ (Fig 4b) coatings are shown. Three different features that may affect the thermal conductivity in different ways can be distinguished: thin horizontal pores (h) oriented parallel to the coating surface, thin vertical pores (v) oriented perpendicular to the surface, and rounded pores (r). We take a pore as rounded when the length/thickness ratio is lower than 4 ($l/t < 4$). It should also be pointed out that in the Nanox coating some nonmelted particles were found (n). As these particles account for only 1.5-1.6% of the total cross-sectional area, their effect on the thermal conductivity can be neglected. The SEM micrographs were digitalized to quantify the microstructural features by image analysis methods.

Compared to the density of 5.07 g cm^{-3} for the HOSP™, the density of 5.38 g cm^{-3} measured for the Nanox coating is slightly higher. Table 2 shows the volume fraction of porosity in the Nanox and HOSP™ samples calculated considering that the density of the fully dense 7Y-PSZ is 6.07 g cm^{3}. The precision of the density measurement was approximately ±0.05 g cm^{3}, which corresponds to an uncertainty in the volume fraction of ±0.01. The total porosity volume fraction and the volume fraction of each of the three types of pores, along with other parameters measured by image analysis, are given in Table 2. The uncertainty in the image analysis results was also approximately ±1%. The porosity as measured by image analysis is lower than the porosity measured by the immersion method in both coatings. This difference can be attributed to the presence of small pores, which could not be resolved in the images used for image analysis. The porosity of the HOSP™ coating is marginally, but consistently, higher than the Nanox coating. The total porosity is not the only factor that affects the thermal conductivity, and a detailed analysis of the pore shape and size should be considered (Ref 7, 8). Of note is that the average length of the thin horizontal pores along the splat boundaries is larger in the HOSP™ coatings, a feature of HOSP™ coatings that has previously been identified (Ref 7, 8).

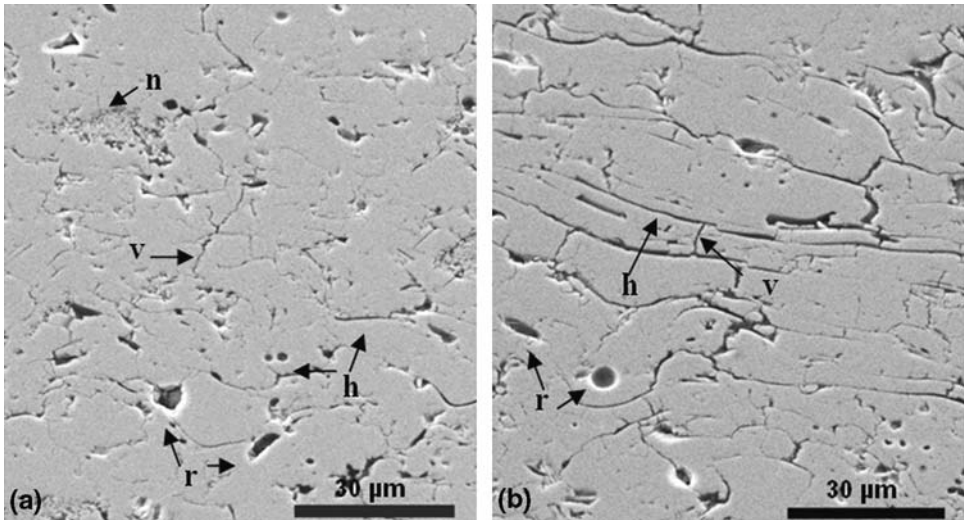

Fig. 4 SEM micrographs of polished cross section of Nanox (a) and HOSP^{TM} (b) coatings where (h) are thin horizontal pores, (v) thin vertical pores, (r) rounded pores, and (n) nonmelted particle

Table 2 Quantitative microstructural features from image analysis characterization of the coatings

Microstructural parameter	Symbol	Nanox	HOSP^{TM}
Water immersion porosity fraction	P_w	0.11	0.16
Total porosity fraction (Image Analysis)	P	0.09	0.11
Porosity fraction for horizontal pores	P_h	0.03	0.04
Porosity fraction for vertical pores	P_v	0.03	0.03
Porosity fraction for spherical pores	P_r	0.03	0.04
Length of horizontal pores (μm)	L	5.8	6.5
Thickness of horizontal pores (μm)	T	0.3	0.3
Average aspect ratio of horizontal pores	l/t	19	22

Figure 5 shows the thermal diffusivity of Nanox, HOSP^{TM}, and mild steel specimens as a function of temperature. The thermal diffusivity values obtained on heating and cooling agree within the accuracy of the technique, indicating that there was no densification up to 800 °C. This result was expected as densification of Y-PSZ plasma sprayed coatings has been reported not to occur at temperatures below 900 °C (Ref 24).

The thermal conductivity data calculated from Eq. 4, averaging the thermal diffusivity values obtained in the heating and cooling cycles, are plotted in Fig. 6. The thermal conductivity of a dense 7Y-PSZ sample measured in a previous work (Ref 25) is also plotted for comparison. The thermal conductivity of both coatings is almost independent of temperature, 1.45 and 0.95 Wm^{-1} K^{-1} for Nanox and HOSP^{TM} specimens, respectively. These values are in the same range as for conventional plasma sprayed TBCs reported in the literature (Ref 25-29). In the same graph, the thermal conductivity of both coatings calculated using Eq. 1 is also plotted with dashed lines. These values represent the Maxwell model that considers rounded pores and are quite far from the experimental data. Therefore, the thermal conductivities were calculated from Eq. 3 using the microstructural parameters in

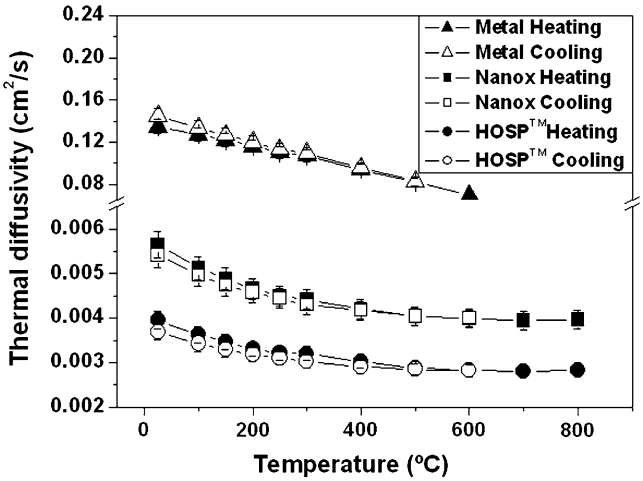

Fig. 5 Thermal diffusivity of Nanox, HOSP^{TM}, and Steel samples for different temperatures

Table 2. The rounded porosity ($l/t < 4$) has been considered as spherical to simplify the calculation. The porosity due to small pores not quantified by image analysis has been estimated as the difference between the porosities obtained by water immersion method and image analysis. This porosity has also been considered as spherical. Although the vertical cracks/pores have not been accounted for, many of them are not totally parallel to the heat flux and may exert some influence on the flux. To simplify calculations, the effects of radiation and the thermal conductivity of the gas that fills the closed pores (assumed to be Argon) have not been considered. These assumptions imply that the values of thermal conductivity obtained with this model are underestimated (Ref 30) over the whole temperature range. The two solid lines in Fig. 6 represent the values obtained with the above

considerations. These values are in good agreement with the experimental data and fit better to the HOSP™ than to the Nanox data at room temperature probably because the porosity is underestimated in the latter due to its nanostructured nature.

On the other hand, the discrepancy in the thermal conductivity temperature dependence between the experimental data and the model cannot be ignored. This discrepancy can be related to the effects of the radiation (Ref 31) and the thermal conductivity of the gas (Argon) that have not been considered in the present model. This different trend leads to an increasing underestimation of the modeled thermal conductivity with temperature observed in Fig. 6.

In Fig. 7, the measured apparent thermal diffusivities of the steel/coating assemblies are compared with the apparent thermal diffusivities calculated, in the way explained above, from the values for the coatings and the metallic substrate shown in Fig 5. The apparent thermal diffusivities can be compared because the thicknesses of steel and coating layers do not differ by more than ~1%.

The differences between the calculated and measured values range from ~7% to ~12%, compared with the coefficient of variation for the measurement technique of 6%, and so we infer the presence of a thermal resistance

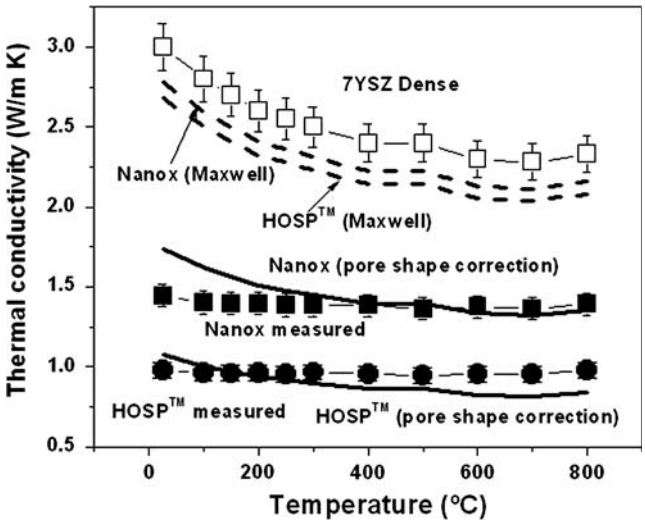

Fig. 6 Thermal Conductivity of Nanox and HOSP™ samples at different temperatures. The solid symbols represent the values obtained using Eq. 4 and the solid lines are the values obtained by Eq 3. Thermal conductivity of dense 7Y-PSZ (Ref 15) and the thermal conductivity obtained with the Maxwell model are also shown for comparison

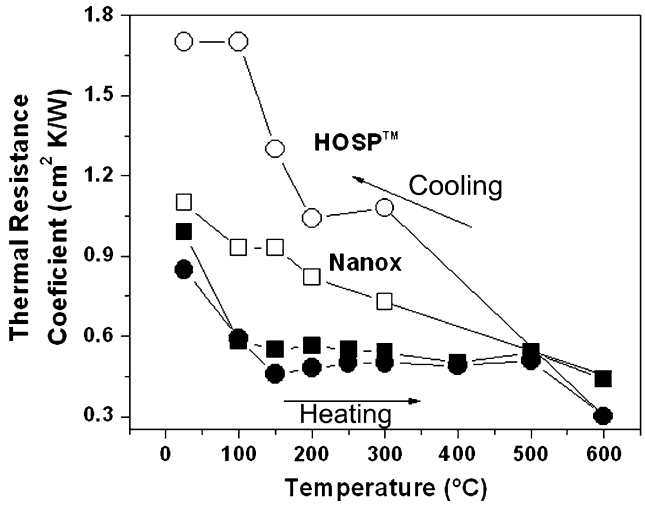

Fig. 8 Calculated thermal resistance coefficient versus temperature for both assemblies. Full symbols are related to the heating cycle and hollow symbols represent the cooling

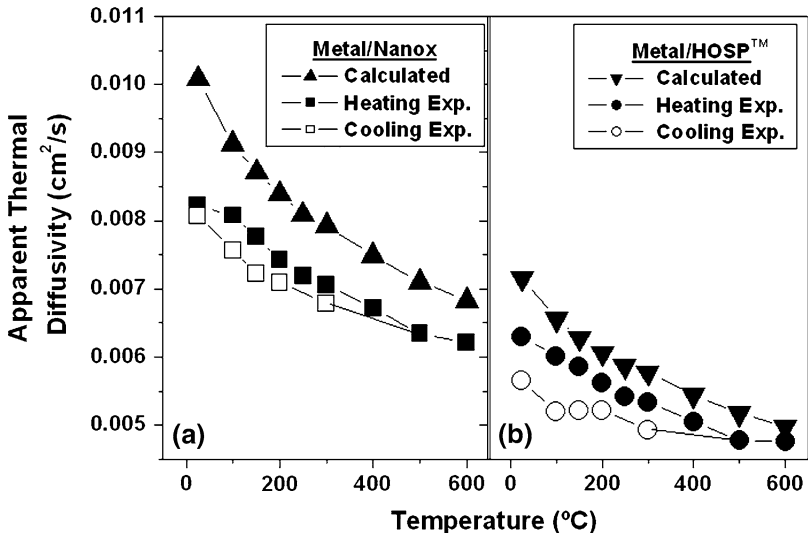

Fig. 7 Calculated and experimental (Exp.) values of apparent thermal diffusivity of layered samples as a function of temperature for Metal/Nanox (a) and Metal/HOSP™ (b) layered structures

between the layers. Figure 8 presents the thermal contact resistance coefficients, as defined in Eq. 6 (Ref 19), calculated for the steel/coating interface as a function of temperature for the heating and cooling ramps. It is of particular interest that the values obtained for the two types of samples during heating are nearly the same. This suggests that the nature of the as-sprayed interface for both coatings is very similar. During the cooling ramp, the thermal contact resistance coefficients increase, especially in the case of the coating produced with the HOSP™ powder, whose thermal contact resistance coefficient at room temperature increases by close to 100%. As diffusivity of the freestanding coatings does not change on cooling (see Fig. 5), no significant alterations in their microstructures are expected. This suggests a change in the nature of the substrate/coating interface. A loss of cohesion between the coating and the substrate may occur due to the residual stresses generated on cooling associated to the mismatch in thermal expansion coefficients, as the value for the steel substrate (11×10^{-6} °C^{-1}) is higher than those of the coatings. In fact, the sample with the lowest thermal expansion coefficient and, therefore, with the highest mismatch exhibits the largest change in interfacial thermal resistance after the thermal cycle. The increase of thermal resistance could be good for thermal insulating properties of the TBC system but it would negatively affect the coating adhesion. Moreover, the presence of a significant and variable interfacial thermal resistance precludes reliable characterization of the thermal properties of the coating while attached to the substrate. However, the thermal diffusivity testing of layered systems could be considered as a tool to analyze the delamination behavior during thermal cycling.

4. Conclusions

Thick Y-PSZ thermal barrier coatings free of macrocracks were air plasma sprayed from two types of commercially available powder. The reduction in the thermal conductivity compared to a dense Y-PSZ is explained only if the shape and size of the pores are accounted for in addition to the volume fraction of porosity. Evaluation of the thermal contact resistance in layered samples suggests that defects may be generated at the coating/substrate interface during thermal cycling. The increase in the thermal contact resistance observed after one thermal cycle depends on the coating thermal expansion coefficient and, therefore, is associated to the stresses developed due to the thermal expansion mismatch between coating and substrate.

Acknowledgments

The authors would like to acknowledge the Auto 21 National Centre of Networks of Excellence and Materials and Manufacturing, Ontario, for financial support, and the Industrial Materials Institute of the National Research Council, Canada, for technical support. Financial support from the MEC-MAT2006-07118 is gratefully acknowledged. E. Garcia acknowledges financial support from the I3P-PC2005L program.

References

1. N.P. Padture, M. Gell, and E.H. Jordan, Thermal Barrier Coatings for Gas-Turbine Engine Applications, *Science*, 2002, **296**, p 280-284
2. D.W. Parker, Thermal Barrier Coatings for Gas Turbines, Automotive Engines and Diesel Engines, *Mater. Des.*, 1992, **13**(6), p 345-351
3. A.G. Evans, D.R. Mumm, J.W. Hutchinson, G.H. Meier, and F.S. Petit, Mechanisms Controlling the Durability of Thermal Barrier Coatings, *Prog. Mater. Sci.*, 2001, **46**, p 505-553
4. P. Ramaswamy, S. Seetharamu, K.B.R. Varma, N. Raman, and K.J. Rao, Thermomechanical Fatigue Characterization of Zirconia (8% Y_2O_3-Zro_2) and Mullite Thermal Barrier Coatings on Diesel Engine Components: Effect of Coatings on Engine Performance, *Proc. Inst. Mech. Eng.*, 2000, **214**, p 729-742
5. M.F. Winkler and D. W. Parker, Thermal Barrier Coatings for Diesel Engines-Ten Years of Experience, *SAE Technical Paper Series*, No. 922438, 1992
6. H. Herman, Plasma Sprayed Coatings, *Sci. Am.*, 1998, **259**(3), p 112-117
7. A. Kulkarni, Z. Wang, T. Nakamura, S. Sampath, A. Goland, H. Herman, J. Allen, J. Ilavsky, G. Long, J. Frahm, and R.W. Steinbrech, Comprehensive Microstructural Characterization and Predictive Property Modeling of Plasma-Sprayed Zirconia Coatings, *Acta Mater.*, 2003, **51**, p 2457-2475
8. Z. Wang, A. Kulkarni, S. Deshpande, T. Nakamura, and H. Herman, Effects of Pores and Interfaces on the Effective Properties of Plasma Sprayed Zirconia Coatings, *Acta Mater.*, 2003, **51**, p 5319-5334
9. J.C. Maxwell, A Treatise on Electricity and Magnetism. Clarendon Press, Oxford, 1904
10. G. Grimvall, *Thermophysical Properties of Materials. Selected Topics in Solid State Physics*, Vol XVIII, North-Holland Physics Publishing, 1986
11. B. Schulzt, Thermal Conductivity of Porous and Highly Porous Materials, *High Temp. High Press.*, 1981, **13**, p 649-660
12. D.P.H. Hasselman, Effect of Cracks on Thermal Conductivity, *J. Appl. Phys.*, 1978, **12**(19), p 403-407
13. B. Shafiro and M. Kachanov, Anisotropic Effective Conductivity of Materials with Nonrandomly Oriented Inclusions of Diverse Ellipsoidal Shapes, *J. Appl. Phys.*, 2000, **87**, p 8561-8569
14. I. Seviostanov and M. Kachanov, Plasma-Sprayed Ceramic Coatings: Anisotropic Elastic and Conductive Properties in Relation to the Microstructure; Cross-Property Correlations, *Mater. Sci. Eng. A*, 2001, **297**, p 235-243
15. K.W. Schlichting, N.P. Padture, and P.G. Klemens, Thermal Conductivity of Dense and Porous Y_2O_3 Stabilized ZrO_2, *J. Mater. Sci.*, 2001, **36**, p 3003-3010
16. I.O. Golosnoy, S.A. Tsipas, and T.W. Clyne, An Analytical Model for Simulation of Heat Flow in Plasma Sprayed Thermal Barrier Coatings, *J. Therm. Spray Technol.*, 2005, **14**, p 205-214
17. A.D. Jadhav, N.P. Padture, E.H. Jordan, M. Gell, P. Miranzo, and E.R. Fuller, Low-Thermal-Conductivity Plasma-Sprayed Thermal Barrier Coatings with Engineered Microstructures, *Acta Mater.*, 2006, **54**, p 3343-3349
18. F. Cernuschi, S. Ahmaniemi, P. Vuoristo, and T.J. Mantyla, Modeling of Thermal Conductivity of Porous Materials: Application to Thick Thermal Barrier Coatings, *J. Eur. Ceram. Soc.*, 2004, **24**, p 2657-2667
19. H.J. Lee, "Thermal Diffusivity in Layered and Dispersed Composites," Ph.D. Thesis, Purdue University, University Microfilm International, 1975
20. R. Soltani, E. Garcia, T.W. Coyle, J. Mostaghimi, R.S. Lima, B.R. Marple, and C. Moreau, Thermomechanical Behavior of

Nanostructured Plasma Sprayed Zirconia Coatings, *J. Therm. Spray Technol.*, 2006, **15**, p 657-662
21. R.E. Taylor and K.D. Maglic, Pulse Method for Thermal Diffusivity Measurement, *Compendium of Thermophysical Properties Measurement Methods. Vol 1, Survey of Measurement Techniques,* K.D. Maglic, A. Cezairliyan, and V.E. Peletsky, Eds., Plenum Press, New York, 1992, p 305-336
22. W. Chi, S. Sampath, and H. Wang, Comparison of the Thermal Transport Property Measurements of Thermally Sprayed Coatings by the Laser and Xenon Flash Techniques, *J. Therm. Spray Technol.*, 2007, **16**, p 444-448
23. R.E. Taylor, X. Wang, and X. Xu, Thermophysical Properties of Thermal Barrier Coatings, *Surf. Coat. Tech.*, 1999, **120-121**, p 89-95
24. F. Cernuschi, L. Lorenzoni, S. Ahmaniemi, P. Vuoristo, and T. Mäntylä, Studies of the Sintering Kinetics of Thick Thermal Barrier Coatings by Thermal Diffusivity Measurements, *J. Eur. Ceram. Soc.*, 2005, **25**, p 393-400
25. J. Wu, X. Wei, N.P. Padture, P.G. Klemens, M. Gell, E. Garcia, P. Miranzo, and M.I. Osendi, Low Thermal Conductivity Rare Earth Zironates for Potential Thermal Barrier Coating Applications, *J. Am. Ceram. Soc.*, 2002, **85**, p 3031-3035
26. S. Ahmaniemi, P. Vuoristo, T. Mantyla, F. Cernuschi, and L. Lorenzoni, Modified Thick Barrier Coatings: Thermophysical Characterization, *J. Eur. Ceram. Soc.*, 2004, **24**, p 2669-2679
27. P. Morrel and R. Taylor, Thermal Diffusivity of Thermal Barrier Coatings of ZrO_2 Stabilized with Y_2O_3, *High Temp. High Press.*, 1985, **17**, p 79-88
28. H.E. Eaton, J.R. Linsey, and R.B. Diwinddie, The Effect Of Thermal Aging on the Thermal Conductivity of Plasma Sprayed Fully Stabilized Zirconia, *Thermal Conductivity 22,* T.W. Tong, Ed., Technomic Pub. Co. Inc., Lancaster, PA, 1994, p 289-300
29. W. Chi, S. Sampath, and H. Wang, Ambient and High-Temperature Thermal Conductivity of Thermal Sprayed Coatings, *J. Therm. Spray Technol.*, 2006, **15**, p 773-778
30. R. McPherson, A Model for the Thermal Conductivity of Plasma Sprayed Ceramic Coatings, *Thin Solid Films*, 1984, **112**, p 89-95
31. A.S. Wagh, Porosity Dependence of the Thermal Conductivity of Ceramics and Sedimentary Rocks, *J. Mater. Sci.*, 1993, **28**, p 3715-3721